The Journal of Chemical Physics ARTICLE scitation.org/journal/jcp

Ultrafast 2DIR comparison of rotational energy transfer, isolated binary collision breakdown, and near critical fluctuations in Xe and SF_6 solutions

Cite as: J. Chem. Phys. 157, 174305 (2022); doi: 10.1063/5.0118395
Submitted: 4 August 2022 • Accepted: 14 October 2022 •
Published Online: 1 November 2022

Matthew C. Rotondaro,[1] Arkash Jain,[1] Shyamsunder Erramilli,[2] and Lawrence D. Ziegler[1,a)]

AFFILIATIONS

[1] Department of Chemistry and the Photonics Center, Boston University, Boston, Massachusetts 02215, USA
[2] Department of Physics and the Photonics Center, Boston University, Boston, Massachusetts 02215, USA

[a)] Author to whom correspondence should be addressed: lziegler@bu.edu

ABSTRACT

The density dependence of rotational and vibrational energy relaxation (RER and VER) of the N_2O ν_3 asymmetric stretch in dense gas and supercritical Xe and SF_6 solutions for near critical isotherms is measured by ultrafast 2DIR and infrared pump–probe spectroscopy. 2DIR analysis provides precise measurements of RER at all gas and supercritical solvent densities. An isolated binary collision (IBC) model is sufficient to describe RER for solvent densities ≤ ~4M where rotational equilibrium is re-established in ~1.5–2.5 collisions. N_2O RER is ~30% more efficient in SF_6 than in Xe due to additional relaxation pathways in SF_6 and electronic factor differences. 2DIR analysis revealed that N_2O RER exhibits a critical slowing effect in SF_6 at near critical density ($\rho^* \sim 0.8$) where the IBC model breaks down. This is attributable to the coupling of critical long-range density fluctuations to the local N_2O free rotor environment. No such RER critical slowing is observed in Xe because IBC break down occurs much further from the Xe critical point. Many body interactions effectively shield N_2O from these near critical Xe density fluctuations. The N_2O ν_3 VER density dependence in SF_6 is different than that seen for RER, indicating a different coupling to the near critical environment than RER. N_2O ν_3 VER is only about ~7 times slower than RER in SF_6. In contrast, almost no VER decay is observed in Xe over 200 ps. This VER solvent difference is due to a vibrationally resonant energy transfer pathway in SF_6 that is not possible for Xe.

I. INTRODUCTION

A detailed, molecular level understanding of rotational and vibrational energy relaxation (RER and VER) dynamics in high density gases and supercritical fluids (SCFs) is of fundamental importance for maximizing reaction outcomes and providing a better molecular level understanding of how equilibrium is established in these dynamic, heterogeneous solution environments. Dense fluids at high temperatures and pressures are solvent environments where many combustion reactions occur. For example, internal combustion engines often operate in a supercritical regime.[1–3] Furthermore, the unique and readily tunable solvation properties of SCFs offer the possibility for selective control of chemical processes and have been successfully exploited in a wide range of applications.[4–10] They also offer the "green" potential to replace organic solvents, thus mitigating negative environmental and human health consequences of those solvents. The experimental studies described here are part of our recent ongoing effort to develop the capabilities of ultrafast two-dimensional infrared (2DIR) spectroscopy to learn about the effects of critical fluctuation dynamics, the onset of liquid character, and the density dependence of rotational and vibrational energy relaxation in near critical solutions.[11,12]

Rotationally inelastic collisions alone can have a profound influence in a wide variety of gas phase phenomena, such as bulk level viscosity, compressibility, and thermal conductivities, in fields ranging from terrestrial and planetary atmospheric chemistry to laser physics and combustion analysis.[13–16] Much of what is known about gas phase rovibrational reaction dynamics has

come from state-to-state, time-resolved spectroscopic measurements necessarily in relatively low-density, homogeneous systems where discrete rovibrational spectroscopic features, in particular, are resolvable.[13,17–25] Other experimental methods for determining rotational relaxation include analysis of acoustics, shock waves, thermal transpiration, and molecular beam experiments. Aside from the indirect nature of most of these approaches, such measurements have been generally restricted to relatively low pressure regimes or neat fluids.[19,21,26–28] Additionally, picosecond scale angular momentum relaxation rates in dense fluids have been derived from nuclear magnetic resonance (NMR) spin relaxation measurements.[29–33] However, rotational *energy* relaxation (RER) or transfer rates in dense media remain difficult to directly assess in liquid-like high density solutions due to the concomitant spectral broadening accompanying spectroscopic features in such molecular environments.

A variety of experimental effects have also been employed to study solvation, broadly defined, in the critical point region of solutions and have been previously reviewed.[4,34] Spectroscopic methods include solvatochromatic peak frequency shifts[34–47] and spectral line shapes[35,42,46,48] in frequency domain measurements and excited state lifetimes[39,44,49–55] and rotational anisotropy determinations[56–58] in time-domain approaches. Although these solvation effects have shown some dependence on the solute–solvent species selected, a phenomenon often observed in dense gas and SCF neat and infinitely dilute solutions is that of a three-regime behavior with respect to solvent density dependence.[34,36,39,47,49,50] For isotherms close to the critical temperature, T_c, the spectroscopic observable or response scale with solvent concentration in the more gas-like density region then appears to plateau near the critical point ($\rho \sim 0.5\rho^*$) before the property again resumes a solvent concentration dependence at more liquid-like densities ($\rho \sim 1.5\rho^*$) although this density dependence may be different than in the gas-like phase. Universal critical point behavior offer several effects that can influence solvation in SCF solutions. The development of long-range spatial correlations, dramatic increase in compressibility, growth in number density heterogeneity, and slowing of density fluctuations are all phenomena evident in near critical fluids ($T \sim 1.01T^*$, $0.5\rho^* \leq \rho \leq 1.5\rho^*$) and are interrelated properties that can provide a basis for understanding solute–solvent interactions and their density dependence in near critical solutions.

In most SCF spectroscopic studies, the observed density dependence is ascribed to local density enhancement or augmentation (LDA).[4,34,42,59–62] Within this framework, the plateau region of the three-regime dependence is enabled by the SCF's large compressibility as the critical point is approached ($\rho \sim 0.5\rho^*$), resulting in a local density in the vicinity of a probe that is larger than the bulk density value. Subsequent changes in bulk density do not alter this local density significantly and a soft or flat density dependence is observed until the bulk density begins to exceed the local density ($\rho \sim 1.5\ \rho_c$).[63] An alternative explanation for the density independence in this near critical region was developed for observed vibrational lifetime (T_1) effects of the CO stretching mode of $W(CO)_6$ in SCFs, highlighting the role of other critical phenomena.[39] In this theoretical treatment, a cancellation of density dependent structural and thermodynamic fluid properties formally results in nearly density independent vibrational lifetimes in the near critical region.[44,50,51] While the universality of this treatment results from the long-range correlations of density fluctuations, the time dependence of these fluctuations was not explicitly considered in this theoretical vibrational energy relaxation (VER) analysis.

Both static and dynamic properties of these density fluctuations may influence solvation in near critical solutions. As the density correlation length increases, there is a corresponding increase in the density correlation relaxation time at the critical point that is described as critical slowing. Analysis of dynamic light scattering[64,65] and small-angle x-ray scattering (SAXS)[66] at accessible angles provides experimental evidence of the density fluctuation rate decrease and how it follows the increase of the spatial correlation length in the near critical region. Simulations have also demonstrated the effect of this critical slowing on local solvation timescales.[67,68] While anomalous density dependent spectral shifts and line shape broadening effects consistent with local density augmentation are evident in the critical region of these solutions, such measurements do not directly reveal dynamical information. 2DIR experiments, in contrast to vibrational lifetime measurements, provide a direct measure of solvent fluctuation timescales as demonstrated here via measurements of the rotational transition frequency–frequency correlation function (FFCF) decays.[11]

Exploiting the recent characterization of 2DIR spectroscopy of quasi-free quantum rotors,[11] we have demonstrated that 2DIR analysis directly provides rotational ($|J|$) energy relaxation (RER) or transfer times in dense gases and SCFs on the subpicosecond to picosecond timescale. 2DIR echo-like properties can be exploited to separate the dynamics of sample members where J is a "good quantum number," i.e., the gas-like quasi-free rotor population, from the ensemble component that is in liquid-like, hindered rotor solvation environments. As described in detail previously,[11,12] the unique spectroscopic signature identifying free rotors in a sample is an anti-diagonal feature in both the ground state bleach/stimulated emission (GSB-SE) and the excited state absorption (ESA) contributions to the 2DIR spectrum. The interpulse, waiting time (T_w) dependence of the perfectly anticorrelated diagonal and anti-diagonal spectral components is a measure of this system's return to rotational equilibrium.[11] The capabilities of this methodology have been demonstrated for the analysis of the N_2O ν_3 asymmetric stretching mode (~2220 cm^{-1}) in gaseous, supercritical, and liquid SF_6 solutions (0.16 < SF_6 ρ^* < 1.87; $\rho^* = \rho/\rho_c$) at $1.01T_c$ as a function of SF_6 density.[12] SF_6 is a simple fluid with a readily accessible critical point (T_c = 318 K, P_c = 48.8 atm), and the large N_2O ν_3 $0 \rightarrow 1$ extinction coefficient ($\varepsilon \sim 1.5 \times 10^3$ M^{-1} cm^{-1}) and relatively long ν_3 lifetime (T_1)[69,70] facilitate these 2DIR measurements. The corresponding VER rates in these solutions are determined by IR pump–probe measurements. Furthermore, density dependent VER analysis is not complicated by the contribution of purely intramolecular relaxation pathways for such a small molecular probe (N_2O). Aside from these desirous experimental attributes, N_2O is an important species in atmospheric chemistry contributing to ozone depletion and a resulting common product of fossil fuel combustion.[71,72] N_2O is currently the second most abundant nitrogen containing compound in the atmosphere and its concentration in the atmosphere is rapidly increasing.[73] Thus, accurate energy relaxation rates and cross sections are central to modeling fundamental collisional N_2O processes in these environments. The previous ultrafast 2DIR results[11,12] revealed efficient N_2O–SF_6 rotational energy transfer rates (rotational equilibrium re-established via just one to two

collisions), offered preliminary dynamical evidence for critical slowing phenomena, and identified the coexistence of gas- and liquid-like sub-ensembles in both the dense gas and SCF phase regions for the solute N_2O in SF_6 solutions. Such details are essentially inaccessible by other experimental optical approaches, especially regarding direct measures of solute–solvent fluctuation timescales. Following our prior 2DIR treatment of free rotors,[11] recent descriptions of the polarization dependence of these responses have been reported.[74–76]

Here, we report a density dependent ultrafast 2DIR spectral analysis and pump–probe measurements of N_2O in Xe solutions along a near critical isotherm ($T^* = 1.005$) and compare the determined N_2O ν_3 RER and VER rates to the corresponding results in SF_6 solutions. 2DIR and pump–probe measurements at two new additional SF_6 solution state points ($\rho^* = 1.17$ and 1.51) are included here to provide a better description of dynamics near the SF_6 critical point region. Some relevant physical and thermodynamic properties of these two solvents are summarized in Table I. SF_6 and Xe are both non-dipolar, spherically shaped molecules with similar masses, critical temperatures, Lennard-Jones potential depths (ε), and polarizabilities (α) in addition to easily accessible critical points (Table I). Differences in some other molecular properties could, however, potentially play a more significant role in the solvation properties of these two solvents/baths. For example, the hard sphere or van der Waals diameter of Xe is 75%–80% smaller than that of SF_6 (Table I) and the critical density of Xe (8.40 M) is ~65% larger than the density of SF_6 at its critical point (5.09 M). Other differences that could affect the solvation or energy transfer dynamics in these two solvents are that Xe lacks internal degrees of freedom and, although both are non-dipolar, SF_6 has a permanent hexadecapole moment.

The goal of these studies is to learn how this 2DIR based approach can be exploited to address some fundamental questions regarding solvation dynamics in these two solvents in the gas to liquid density regime. Specific topics of interest here include the adequacy and breakdown of isolated binary collision (IBC) descriptions for rotational and vibrational energy transfer, dynamical critical phenomena effects on solvation interactions, and evidence of simultaneous gas/liquid fluid heterogeneities at the near critical densities of these fluids.

TABLE I. Comparison of some Xe and SF_6 thermodynamic and physical properties.

Property	Xe	SF_6
T_c (°C)	16.6	45.6
P_c (atm)	57.7	37.1
MW (g/mol)	131	146
ρ_c (M)	8.40	5.09
χ_c[a]	0.291	0.360
σ (Å)[b]	4.047	5.128
ε/k (K)[b]	231.0	222.1
B_2 (L/mol)	−0.122	−0.207
α (nm^3)[108,109]	4.0×10^{-3}	4.5×10^{-3}

[a]Critical compressibility factor $\chi_c = P_c V/nRT_c$.
[b]Lennard-Jones constants determined from experimental viscosity data.[110]

II. EXPERIMENTAL

The experimental setup has been described in detail previously.[11,12] Briefly, all 2DIR spectra were collected in a pump–probe configuration using perpendicularly polarized 85 fs IR pulses (FWHM ~ 300 cm^{-1}) centered at ~2200 cm^{-1}. These relative polarizations were chosen to minimize background scattering contamination contributions to the 2DIR spectra. The expanded IR beams were focused onto the sample by a parabolic mirror to a diameter of ~100 μm. The phase-matched, heterodyne-detected signal in the probe direction was dispersed in a monochromator and detected by a double-array 32 element cryogenically cooled MCT detector (Infrared Associates, Inc.) with a resulting spectral resolution along the 2DIR ω_3 axis of 3 cm^{-1}/pixel. The resolution along the 2DIR ω_1 axis is determined by Fourier transform treatment and is ~0.1 cm^{-1}. N_2O, SF_6, and Xe gases of the highest available purity (>99.8%) were compressed by a pressure generator into a stainless-steel cell with a 100 μm optical path length between two 2 mm thick z-cut sapphire windows. All solutions were allowed to equilibrate for ~24 h before any measurement was performed. Proportional integral derivative (PID) control was used to regulate and maintain sample cell temperatures to within ±0.1 °C and a transducer gauge ensured that sample pressures were constant within a precision of ±1 psi. Relative sample densities were derived from the NIST online database.[77]

One-color, magic angle, dispersed pump–probe responses were obtained on the same 2DIR setup with one of the pump beams blocked and are reported as the change in sample optical density, $\Delta OD(t)$, of the dispersed probe beam in the absence and presence of the pump, as a function of the interpulse delay. The longest delay time reported here, 200 ps, is limited by our current scanning stage capabilities. Experimental uncertainties for the reported VER rates ($1/T_1$) are given by best-fit determined 95% confidence limits. FTIR absorption spectra were collected at 0.125 cm^{-1} resolution. A small flat baseline correction (<1% OD maximum) to account for sapphire window transmission was applied to all displayed absorption spectra. The maximum absorbance of the N_2O sample solutions was in the range of ~0.3–0.5 OD for all 2DIR and pump–probe measurements.

III. RESULTS

A. Vibrational absorption spectral shapes

FTIR spectra of the N_2O ν_3 asymmetric stretching mode in Xe solvent with densities spanning gas, SCF, and liquid phases ($0.10 \leq$ Xe $\rho^* \leq 1.55$) are shown in Fig. 1 for a $T^* = 1.005$ isotherm (18.0 °C). The low solute concentration of these solutions (≤1% N_2O) ensures all intermolecular interactions contributing to the measurements in these studies are in the infinite dilute solution limit. The N_2O ν_3 density dependent spectral line shapes in Xe (Fig. 1) are similar to those observed for N_2O ν_3 in dense SF_6[11,12] (see Fig. S1). Pressure-broadened, unresolved N_2O P ($\Delta J = -1$) and R ($\Delta J = +1$) rovibrational branches, centered at ~2211 and ~2237 cm^{-1}, respectively, are clearly identifiable at gaseous Xe state points where $\rho^* \leq 0.37$ (3.11 M). The Q-branch ($\Delta J = 0$) for this parallel-type vibrational band is formally symmetry-forbidden for the free rotor[78] and thus is not evident in the low solvent density spectra ($\rho^* <$ ~0.3). However, as the Xe solvent density increases

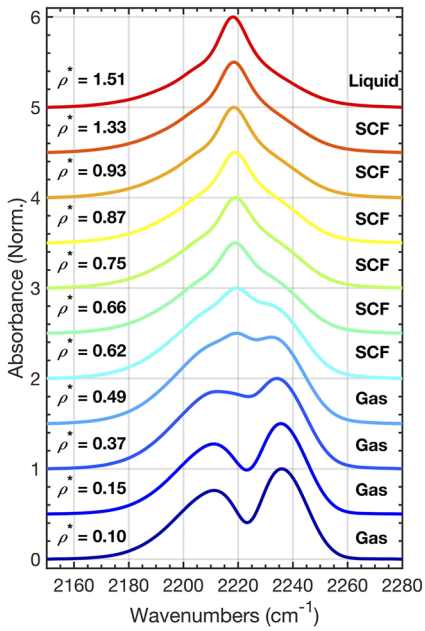

FIG. 1. Normalized FTIR absorption spectra of the N_2O ν_3 asymmetric stretch mode in Xe as a function of solvent reduced density (ρ^*). Xe (T, P, ρ) state points range from gas to supercritical fluid (SCF) at 18 °C (1.005Tc) and the liquid at 14 °C (0.99 Tc).

beyond $\rho^* \sim 0.4$, the ν_3 band shape exhibits a growing additional "Q-branch-type" pure vibrational $0 \rightarrow 1$ ν_3 transition feature centered at ~2219 cm^{-1}, and the P and R branches become increasingly less pronounced. At Xe densities greater than $\rho^* \sim 0.7$ corresponding to SCF state points, the N_2O ν_3 P and R branches are barely visible residual "shoulders" to the red and blue of the stronger central, Q-branch-like feature. At the highest solvent densities shown in Fig. 1, Xe $\rho^* \geq 0.87$, these $\Delta J = \pm 1$ branches are no longer identifiable. Interestingly, the N_2O ν_3 absorption spectra in liquid Xe ($\rho^* = 1.55$) at a temperature just below T_c (14 °C, $T^* = 0.99$) and in the highest supercritical Xe densities ($\rho^* \geq \sim 0.9$) (Fig. 1) exhibit a band shape dominated by Lorentzian character and are nearly identical. In contrast, only the N_2O ν_3 absorption spectrum in liquid, not supercritical SF_6 ($\rho^* = 1.87$, $T^* = 0.93$),[12] exhibits a nearly Lorentzian band shape (Fig. S1).[12] A small shoulder at ~2207 cm^{-1} corresponding to the N_2O ν_2 (589 cm^{-1}) hot band ($\nu_2 \rightarrow \nu_2 + \nu_3$) absorption is also evident in the liquid Xe spectrum (Fig. 1), and it has been noted in previous N_2O ν_3 spectra in liquid SF_6 and other solvents also.[11,12,79,80]

Although the N_2O ν_3 absorption band shapes in Xe (Fig. 1) and SF_6[12] (Fig. S1) are very similar and exhibit analogous solvent density dependent band shape changes for these near critical isotherms, some phenomenological differences are evident. Most spectroscopic probes of SCF solvation effects are reported as a function of reduced density such as ρ^* (ρ/ρ_c), placing such descriptions in the context of universal scaling properties that, in part, define the thermodynamic and statistical characteristics of near critical behavior.[81] However, N_2O ν_3 absorption spectra in Xe and SF_6 display distinctly different line shapes for comparable ρ^* (see Fig. S2). For example, the ν_3 line shapes in Xe $\rho^* = 0.66$, 0.87, and 1.33 are qualitatively different than in the corresponding $\rho^* = 0.67$, 0.86, and 1.36 SF_6 spectra, respectively. Qualitatively, the central Q-branch-like or pure vibrational feature is a more intense absorption feature at lower ρ^* in Xe as compared to the same reduced SF_6 density. In contrast, the N_2O ν_3 absorption band shapes are quite similar when Xe and SF_6 solution absorption spectra of comparable *absolute* number densities, i.e., solvent molarities, are compared. N_2O ν_3 absorption spectra in Xe $\rho^* = 0.37$, (gas), 0.62 (SCF), and 1.33 (SCF) corresponding to 3.1, 5.2, and 11.2 M Xe solutions closely resemble the spectra in SF_6 $\rho^* = 0.67$ (SCF), 0.99 (SCF), and 1.87 (ℓ) or equivalent SF_6 molarities of 3.4, 5.1, and 9.6 M, respectively. This result is understandable for these similarly sized solvents given that ρ_c for Xe (8.40 M) is 65% larger than for SF_6. Phenomenologically, for the same ρ^*, the solvent with the larger ρ_c shows the more dominant central Q-branch-like IR absorption features, at least for these N_2O solutions. Aside from these phenomenological vibrational line shape comparisons, potentially other aspects of the solvation dynamics may be more dependent on the solvent number density than on the relation to ρ_c, i.e., ρ^*, as discussed below. Finally, while these strongly density dependent absorption spectra indicate substantial solvation changes in this gas to liquid solvent transition region, nonlinear optical measurements are required to reveal evidence of free N_2O rotor populations, to provide quantitative measures of distinct rotational and vibrational energy relaxation rates, and to address the adequacy of IBC relaxation dynamics in these high density and supercritical solutions.

B. Vibrational peak shifts

As indicated above, solvatochromatic vibrational peak shifts have been used as a measure of a solute's local solvent density and taken as evidence for local density augmentation in the near critical region of SCFs. Generally a red shift is observed as solvent density increases, consistent with both dielectric continuum and molecular based theoretical treatments.[34,37,38,45,46,82–84] In most, but not all, solute–solvent systems, the density dependent vibrational peak shift exhibits a plateau in the near critical ($\rho^* \sim 0.8$–1.2) density region along isotherms very close to T_c.[35,37,39,42–44]

For completeness in reporting on the density dependence of spectroscopic signatures in Xe and SF_6 solution isotherms, the solvatochromatic N_2O ν_3 vibrational peak shift as a function of solvent molarity derived from Fig. 1 (Xe) and Fig. S1 (SF_6) absorption spectra is shown in Fig. 2. For the weakly dipolar N_2O solute in the non-dipolar solvents, Xe or SF_6, no Q-branch, liquid-like feature is evident in the ν_3 absorption spectra at low solvent concentrations, i.e., <~4M in contrast to previous vibrational peak shift studies. However, a small absorption band between the dominant P and R branches at ~2020 cm^{-1} attributable to N_2O in local liquid-like, hindered rotor environments first becomes detectable in Xe and SF_6 solutions at 4.1 and 4.4 M, respectively, and then increases in magnitude as the solvent density increases. These nearly identical solvent number densities correspond to distinctly different reduced densities: $\rho^* \sim 0.49$ (Xe) and 0.86 (SF_6). Only a very small ~1 cm^{-1} frequency shift is observed over the reported limited density range and the highest density point in this plot (Fig. 2) corresponds to the liquid solution as indicated. Thus, this commonly employed measure of SCF solvation does not appear to be

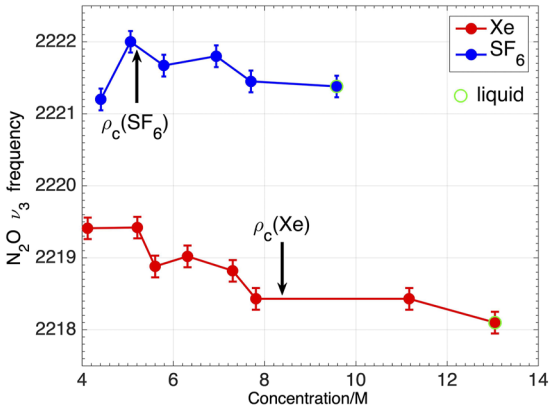

FIG. 2. Frequency shift of the N_2O ν_3 Q branch-like, hindered rotor FTIR feature as a function of SF_6 and Xe concentration corresponding to Fig. 1 (Xe) and Fig. S1 (SF_6) spectra. The vertical arrows indicate the SF_6 or Xe critical density molarity. The highest density point (green circle) for each solvent corresponds to a liquid $T^* = 0.92$ (SF_6) or 0.99 (Xe) solution. The absorption intensity of this feature is just detectable at ~4M and increases with solvent density.

very informative for the solution systems of interest here. The peak frequency difference on going from Xe to SF_6 is consistent with trends observed for this vibrational transition in more polarizable solvent environments[85,86] and is much larger than the observed density dependence over this density regime. Nonetheless, even given this very small peak shift, limited density range, and small absorption size when first evident, the ν_3 peak frequency in Xe and SF_6 exhibits only a very small red shift with density. While arguably the density dependence of the N_2O ν_3 peak frequency in Xe hints at a weak three-regime behavior with a plateau near the critical point as observed in other SCF IR studies, greater precision data at additional near critical state points are needed to confirm that small magnitude trend in this system. Surprisingly, a peak blue shift is observed on going from 4.41 M, $\rho^* = 0.87$, the first density where the liquid-like absorption feature is just barely detectable in SF_6, to 5.06 M, $\rho^* = 0.99$, and it may have resulted from the solvent concentration dependent distribution of density inhomogeneities near the critical point offering both higher and lower SF_6 density environments for N_2O.[45,87] The ability to unequivocally detect and identify a small Q-branch-like N_2O ν_3 vibrational feature in the 4.4 M ($\rho^* = 0.86$) SF_6 solution is shown in Fig. S3. Subsequent MD simulations and some additional data points will address this observation in future works. Note that these frequency shifts (Fig. 2) reflect ensemble averaged measures of solvation for the hindered rotor population in the sample ensemble and do not directly report on the quasi-free rotors giving rise to the 2DIR RER decays discussed below (*vide infra*).

C. 2DIR spectra

2DIR spectra were acquired for each of the dilute N_2O in Xe solutions whose ν_3 absorption spectra are shown in Fig. 1 as a function of waiting times, i.e., fixed delay time (T_w) between the second and third IR pulses.[11] In addition, 2DIR spectra of N_2O in some additional higher density SF_6 state points not previously observed ($\rho^* = 1.17$, $\rho^* = 1.51$) are also reported here. Three representative N_2O ν_3 2DIR spectra in Xe solutions with reduced densities $\rho^* = 0.10$ (gas), 0.49 (gas), and 0.93 (SCF) as a function of three T_w's are shown in Fig. 3 (see the supplementary material, Figs. S4–S12 for all additional 2DIR spectra). The short time ($T_w \sim 0.150$ ps), low-density N_2O/Xe spectra closely resemble our previously reported N_2O/SF_6 spectra.[11,12] They consist of two distinct, oppositely signed elongated "X"-shaped spectral features due to a ground state bleach and stimulated emission (GSB-SE) signal (red) and an excited state absorption (ESA) signal red-shifted along ω_3 due to the ~28 cm^{-1} anharmonicity of the $1 \rightarrow 2$ transition (blue). As T_w increases for a given solvent density, each of these spectral features becomes more compact and symmetrical in shape (Fig. 3). With increasing solvent density, the initial "X" patterns become less distinct, consistent with faster relaxation (*vide infra*). While elongated spectral features along the diagonal ($\omega_1 = \omega_3$) are characteristic of an inhomogeneously broadened resonant transition in condensed phase 2DIR spectra,[88] the diagonal (along or parallel to $\omega_1 = \omega_3$) and *anti-diagonal* (~perpendicular to $\omega_1 = \omega_3$) GSB-SE or ESA intensity features in the 2DIR spectra of free rotors arise from the $\Delta J = \pm 1$ absorption selection rule for rovibrational transitions (parallel polarized band). Thus, phenomenologically, evidence of elongated anti-diagonal character is the key 2DIR spectral feature that identifies quasi-free rotor population in a sample ensemble.[11,12]

Modeling the fluctuation dynamics of these rovibrational spectral features as a stochastic process characterized by an exponentially decaying transition frequency–frequency correlation function (FFCF), $\langle \delta\omega(t)\delta\omega(0)\rangle$, yields a J-scrambling or RER time (τ_c) describing how rapidly the rotational degrees of freedom of the resonant system return to thermal equilibrium.[11,12] The T_w dependence of these diagonal and anti-diagonal rovibrational 2DIR spectral features is used to determine τ_c at each solvent state point via the center line slope (CLS) methodology.[89] 2DIR determined and the corresponding best-fit CLS decays are shown in Fig. 3 for these representative spectra. The CLS slope values that start at positive/negative values at the shortest T_w times and then decay to ~0 correspond to fluctuation dynamics evident from the diagonal/anti-diagonal 2DIR features.[11] (CLS decays and best-fits for all studied state points are given in the supplementary material, Figs. S4–S12). 2DIR CLS decays at all Xe and SF_6 state points are well-fit by a single exponential decay time, τ_c, and a small (~5%), positive constant offset. The contribution of liquid-like or hindered rotor N_2O solute species where J is no longer a good quantum number appears near the center of these "X" GSB-SE and ESA features and will grow in intensity as the density increases, paralleling the concentration dependence of the central feature of the absorption spectra (Figs. 1 and S1). However, by excluding these central regions from the CLS analysis, the reported T_w dependence of the CLS decays unambiguously reports on the quasi-free rotor energy relaxation (RER) dynamics of N_2O molecules in the sample ensemble. The small positive CLS offsets do not systematically scale with density or the solvent type (Xe vs SF_6) and do not appear in modeled 2DIR spectra,[11] and they are thus currently attributed to background scattering contributions.

The 2DIR determined timescales of N_2O RER, τ_c, are given in Tables II and III for Xe and SF_6 solutions, respectively. These are averages for the diagonal and anti-diagonal 2DIR T_w dependence at each density. Over the Xe low-density gas to SCF

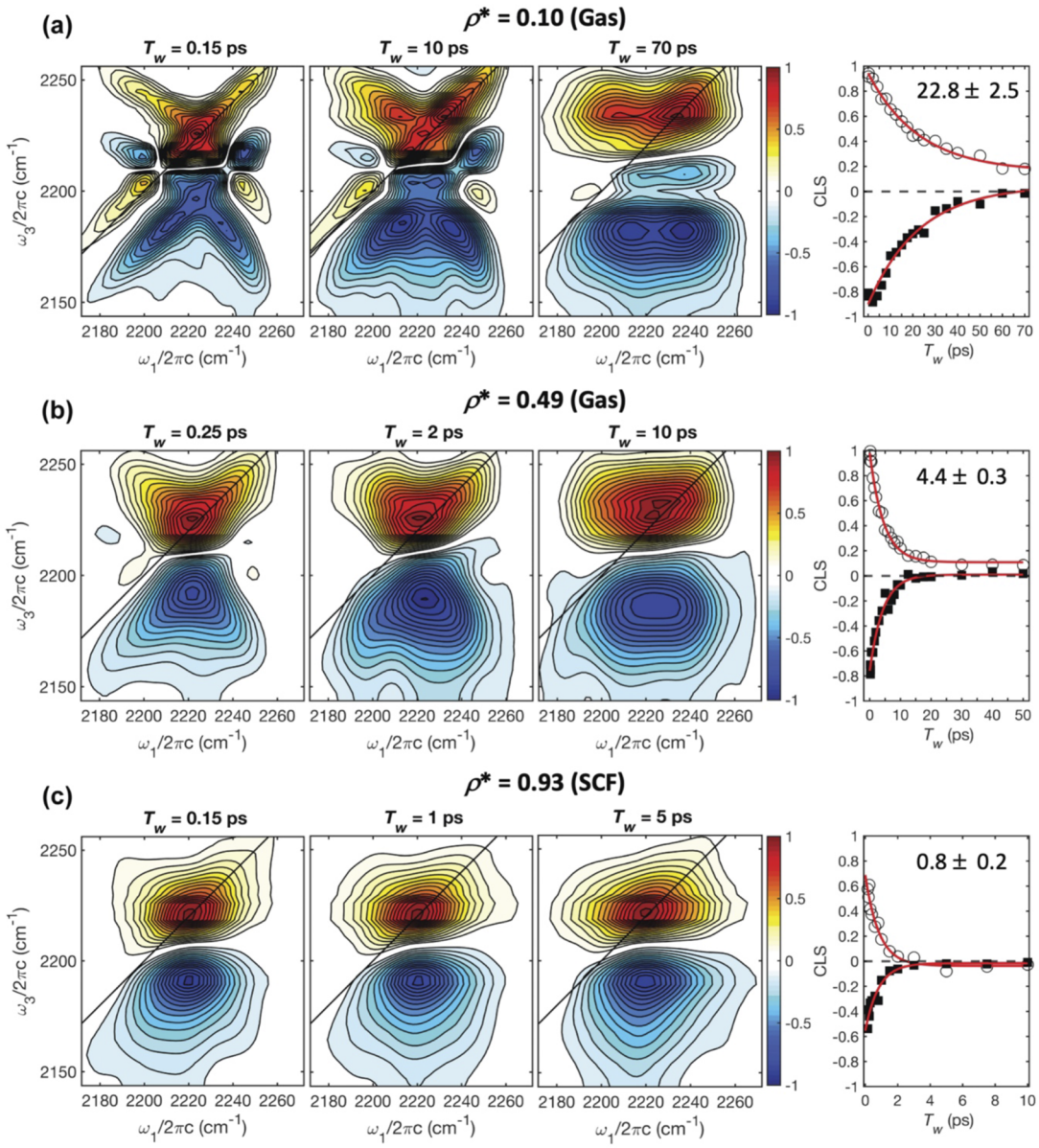

FIG. 3. Representative 2DIR spectra and corresponding CLS decays of the N_2O ν_3 asymmetric stretch fundamental in Xe at three isothermal (T = 18 °C = 1.005T_c) reduced density state points in the gaseous and SCF region: (a) ρ^* = 0.10 (gas); (b) ρ^* = 0.49 (gas); and (c) ρ^* = 0.93 (SCF). 8% intensity contours are shown for all 2DIR spectra. Red contours correspond to the positive-going GSB-SE component and blue contours correspond to the negative-going ESA component red-shifted along ω_3 by the 1-2 vibrational transition anharmonicity (~28 cm^{-1}). See the supplementary material for 2DIR spectra at the other reported Xe state points and two additional N_2O in SF_6 SCF solutions.

ρ^* = 0.10–1.33 range, the RER decay times vary from 22.8 ± 1.8 to 0.7 ± 0.1 ps, decreasing by a factor of ~30. By comparison, in the SF_6 ρ^* = 0.16–1.51 density range, τ_c varies from 9.5 ± 0.5 to 0.9 ± 0.1 ps, decreasing by ~10-fold.

For N_2O in liquid Xe solutions at T = 14 °C (ρ^* = 1.55), no anti-diagonal 2DIR character can be detected at even the shortest T_w (150 fs) time and the 2DIR spectra exhibit no T_w dependence (Fig. 4). Only a typical 2DIR pattern of a fully symmetrized purely vibrational feature is observed for the N_2O/Xe solution at this state point. This observation is consistent with no free N_2O rotors being present in these liquid Xe solvent solutions and the pure vibrational transition dephasing dynamics being in the fast

TABLE II. Summary of experimental and calculated results for N_2O ν_3 mode in Xe at T^* = 1.005 (291.2 K).

Physical state	Pressure (atm)	Xe reduced density, ρ^*	Xe absolute density (M)	τ_c (ps)[b]	τ_{coll} (ps)	Z_{rot} (ps)
Gas	17.3	0.10	0.81	22.8 ± 1.8	10.2	2.2 ± 0.2
	25.1	0.15	1.26	16.8 ± 1.4	6.6	2.5 ± 0.2
	46.9	0.37	3.11	6.6 ± 0.5	2.7	2.4 ± 0.2
	53.3	0.49	4.12	4.4 ± 0.2	2.0	2.3 ± 0.1
	57.0	0.62	5.21	3.0 ± 0.3	1.6	1.9 ± 0.2
SCF	57.7	0.66	5.60	1.9 ± 0.2	1.5	1.3 ± 0.1
	58.5	0.75	6.31	1.2 ± 0.2	1.3	0.9 ± 0.2
	59.0	0.87	7.30	1.0 ± 0.15	1.2	0.8 ± 0.2
	59.2	0.93	7.81	0.8 ± 0.1	1.1	0.7 ± 0.1
	61.0	1.33	11.17	0.7 ± 0.1	0.8	0.9 ± 0.1
Liquid[c]	59.3	1.55	13.05	···	···	···

[a]SCF T > T_c, P > P_c; Gas T > T_c, P < P_c; Liquid T < T_c, P < P_c.
[b]Average of diagonal and anti-diagonal CLS decay constants.
[c]Temperature for liquid Xe 14 °C, T^* = 0.99. No free rotor character detected in 2DIR of liquid solution.

modulation limit where no spectral diffusion is evident.[90,91] Analogously, no free rotor or evidence of spectral diffusion was observed for N_2O in liquid SF_6 solutions at T = 20 °C (ρ^* = 1.87) as well.[12]

These results further demonstrate that 2DIR provides dynamical timescales inaccessible from analysis of the corresponding linear FTIR spectra. For example, the 2DIR determined RER decay time (τ_c) is 1.2 ps in a ρ^* = 0.75 Xe solution, and at ρ^* = 1.33, τ_c = 0.7 ps. The corresponding N_2O ν_3 absorption spectra in Xe (Fig. 1) are nearly identical at these densities although the RER rate changes by nearly a factor of two. Furthermore, 2DIR analysis found no evidence for free rotors in the liquid Xe (ρ^* = 1.55) sample, yet the liquid Xe FTIR spectrum is nearly the same as those for ν_3 absorption in Xe when ρ^* > ~0.75 (Fig. 1).

IV. DISCUSSION

A. Rotational energy relaxation dynamics

N_2O free rotor populations were detectable by 2DIR spectroscopy at all the dense gas and supercritical state points studied in both solvents. The corresponding CLS determined rates ($1/\tau_c$) of N_2O RER in SF_6 and Xe are plotted as a function of solvent concentration (M) and reduced density (ρ^*) in Figs. 5 and 6, respectively. At low solvent densities, a simple IBC model description is found for both Xe and SF_6 solutions. At higher SF_6 densities, the "three-regime" density dependence, often observed in other density dependent spectroscopic studies of SCFs along near critical isotherms, is evident for RER rates in SF_6 (Fig. 5). However, a very different density dependence without a plateau region is observed

TABLE III. Summary of experimental and calculated results for N_2O ν_3 mode in SF_6 T^* = 1.01 (322 K).

Physical state[a]	Pressure (atm)	SF_6 reduced density, ρ^*	SF_6 absolute density (M)	τ_c (ps)[b]	τ_{coll} (ps)	Z_{rot} (ps)	T_1 (ps)[c]	Z_{vib} (ps)
Gas	17.0	0.16	0.82	9.5 ± 0.5	6.7	1.5 ± 0.1	108 ± 8.7	16.1 ± 1.3
	26.0	0.30	1.51	6.0 ± 0.4	3.6	1.7 ± 0.1	39.7 ± 3.3	11.0 ± 0.9
	37.9	0.67	3.43	2.8 ± 0.3	1.7	1.6 ± 0.2	···[d]	···[d]
	38.8	0.86	4.41	2.4 ± 0.2	1.5	1.6 ± 0.1	21.4 ± 2.0	14.2 ± 1.3
SCF	39.1	0.99	5.06	2.3 ± 0.1	1.4	1.6 ± 0.1	16.6 ± 2.1	11.9 ± 1.5
	40.0	1.17	5.79	1.9 ± 0.1	1.0	1.9 ± 0.1	14.7 ± 1.2	14.7 ± 1.2
	41.3	1.36	6.94	1.4 ± 0.1	0.8	1.8 ± 0.1	11.1 ± 1.8	13.9 ± 2.3
	47.0	1.51	7.70	0.9 ± 0.1	0.7	1.3 ± 0.1	11.0 ± 1.7	15.7 ± 2.4
Liquid[e]	22.0	1.87	9.58	···	0.6	···	6.1 ± 0.7	10.2 ± 1.2

[a]SCF T > T_c, $P > P_c$; Gas T > T_c, P < P_c; Liquid T < T_c, P < P_c.
[b]Average of diagonal and anti-diagonal CLS decay constants.
[c]Fastest pump–probe component of a two-component decay fit.
[d]No VER data available for this state point.
[e]Temperature for liquid SF_6 20 °C, T^* = 0.92. No free rotor character detected in 2DIR of liquid solution.

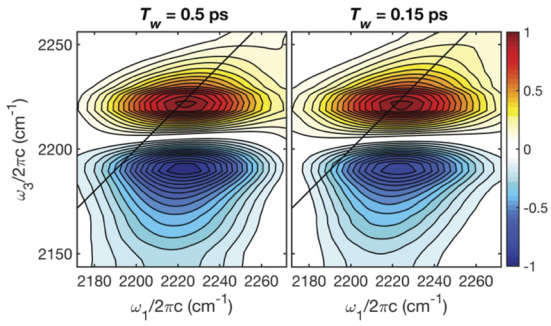

FIG. 4. 2DIR spectra of N_2O in liquid Xe (T = 14 °C, T* = 0.99, ρ^* = 1.87) for two representative waiting times, T_w = 0.15 and 0.5 ps. No free rotor character, i.e., anti-diagonal features and no spectral diffusion dynamics are detectable at this density. Some diagonal (i.e., along $\omega_1 = \omega_3$) scatter is evident at this high-density state point.

for the N_2O RER rate in Xe as the solvent density approaches the critical point (Fig. 6). These collisional dynamics are quantitatively described below.

1. IBC regime

The N_2O RER rates ($1/\tau_c$) are found to be linearly dependent on solvent concentration in the lower solvent density regime for ρ_{SF_6} and ρ_{Xe}. A linear best fit to these 2DIR CLS decays ($1/\tau_c$) at these lowest bath densities is the resulting red dashed line shown in Figs. 5 and 6. Rate constants for N_2O RER (k_{rot}) in the solvent density region adequately described by a simple IBC model given by the slope of these best-fit lines are 1.70×10^{-10} and 8.9×10^{-11} cm^3 s^{-1} molecule^{-1} in SF_6 and Xe, respectively (Table IV). These k_{rot} rate constants in the IBC density regime

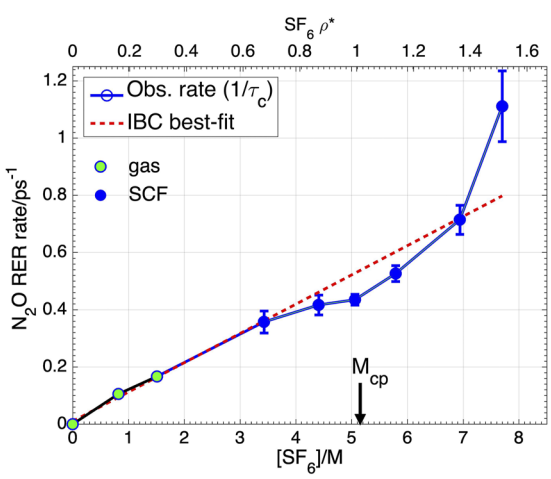

FIG. 5. 2DIR determined N_2O rotational energy relaxation (RER) rates ($1/\tau_c$) as a function of SF_6 concentration (*reduced* density ρ^* at the top and molarity at the bottom scale) for a T* = 1.01 isotherm (48 °C). Arrow indicates SF_6 density at the critical point (ρ_c = 5.01M). Dashed red line corresponds to the result obtained from linear best fit to lowest density rates ([SF_6] ≤ 3.43M). Gas (green, $P < P_c$) and SCF (blue, $P > P_c$) state points are indicated.

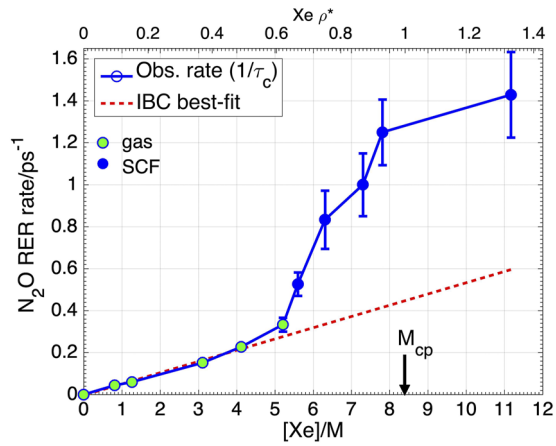

FIG. 6. 2DIR determined N_2O rotational energy relaxation (RER) rates ($1/\tau_c$) as a function of Xe concentration (*reduced* density ρ^* at the top and molarity at the bottom scale) for a T* = 1.005 isotherm (18 °C). Arrow indicates Xe density at the critical point (ρ_c = 8.4M). Dashed red line corresponds to the result obtained from linear best fit to lowest density rates ([Xe] ≤ 4.12M). Gas (green, $P < P_c$) and SCF (blue, $P > P_c$) state points are indicated.

correspond to N_2O RER cross sections (σ_{RER}) of 38.0 (SF_6) and 20.7 (Xe) Å^2/molecule (Table IV). $\sigma_{RER} = k_{rot}/\bar{v}$ and the temperature and mass dependent mean relative velocity is $\bar{v} = (8k_BT/\pi\mu_{AB})^{1/2}$. μ_{AB} is the reduced mass of the A, B collision pair and the other symbols have their usual meaning. Thus, the 2DIR determined N_2O RER rate constant/cross section is nearly a factor of 2 larger in SF_6 than in Xe at their respective experimental state points [$k_{rot}(SF_6)/k_{rot}(Xe)$ = 1.91].

In the *simplest* IBC treatment, the energy transfer rate is just proportional to the product of the density dependent collision frequency and temperature dependent probability per collision. In such a treatment, a hard sphere model analysis can be used to characterize the collisional efficiency of this process and identify some factors that can account for the observed RER rate solvent difference. The collision frequency (s^{-1}), or equivalently the inverse of the mean free collision time ($\nu_{coll} = 1/\tau_{coll}$) between solute A and solvent B at infinite dilution, is given by

$$\nu_{coll} = N_o\rho_B\sigma_{AB}\bar{v}_{AB}, \quad (1)$$

where ρ_B is the solvent molarity, N_o is the Avogadro's number, and σ_{AB} is the geometric cross section approximated by $\sigma_{AB} = \pi d_{AB}^2$

TABLE IV. 2DIR determined rates of N_2O rotational energy relaxation in the IBC region.[a,b]

Solvent	T (K)	k_{RER} (cm^3 s^{-1} molecule^{-1})	k_{RER} (s^{-1} M^{-1})	σ_{RER} (Å^2/molecule)
SF_6	321	1.70×10^{-10}	1.02×10^{11}	38.0
Xe	291	8.90×10^{-11}	5.36×10^{10}	20.7

[a] [SF_6] ≤ ~3.4 M, [Xe] ≤ ~4.1 M.
[b] Estimated k_{rot} uncertainty ±15% given by 95% fitting confidence limits.

where $d_{AB} = r_A + r_B$ is the hard sphere distance between solute (A) and solvent (B) molecular centers.[25] A range of empirically and theoretically based estimates for hard sphere dimensions for N_2O, Xe, and SF_6 can be found in the literature and are summarized in Table V. Here, we take an average of these values to determine d_{AB}. From these parameters and the observed rate constants, N_2O RER in these simple solvents is found to be a rapid and efficient process in the IBC regime corresponding to 1.7 and 2.4 collisions (Z_{rot}) in SF_6 and Xe, respectively, where the 2DIR determined k_{rot} gives $Z_{rot} = \frac{\sigma_{AB}\bar{v}}{k_{rot}}$. Typical $Z_{\rm rot}$ values in the literature range from 1 to 6[21,92–95] and while our data fall in this range, 2DIR analysis provides greater precision in calculating $Z_{\rm rot}$ (Tables II and III).

The 2DIR determined rate constants, k_{rot}, and the corresponding RER cross sections, σ_{RER}, are of the order of previous RER measurements (1–100 Å^2/molecule) given by state-to-state observations[13,17,18,20,25,96] although here they are a measure of the J-averaged rotational population return to thermal equilibrium. However, the 2DIR rates are given for solvent concentrations much greater than possible for state-to-state determinations.

The RER rates and collision partner dependence found by 2DIR may also be more closely compared to the nonoptical measurement of rotational dynamics given by NMR T_1 spin relaxation times. The decay time of the ensemble averaged angular momentum correlation function, τ_J, and the corresponding cross section given by $\sigma_J = (\rho\bar{v}\tau_j)^{-1}$ can be related to the ~millisecond NMR T_1 timescale such that $1/T_1 \propto \tau_J$.[29–33,97–99] Aside from the relative merits of each approach for determining picosecond timescale dynamics, σ_J should be larger than σ_{RER} for a given dilute solute–bath system because both orientational and rotational energy transfer processes contribute to τ_J in contrast to the 2DIR results. Indeed, the value for σ_J reported by NMR studies for N_2O in Xe gas solutions at ~300 K is 65 Å^2/molecule[32] as compared to the value 20.7 Å^2/molecule found by the direct time-domain 2DIR measure of N_2O RER in Xe. Thus, given the disparate experimental timescales, milliseconds (NMR) vs subpicosecond (2DIR), and the additional NMR orientational relaxation contribution, these results are consistent. Furthermore, after correcting for hard sphere diameter differences, NMR analysis found that N_2O J relaxation was ~14% more efficient in SF_6 than in Xe. This is consistent with the 2DIR trend uncovered here. Furthermore, the values for σ_J given by NMR spin relaxation measurements are 50.0 and 30.8 Å^2/molecule for CO, another small dipole molecular probe (CO 0.12 D, N_2O 0.16 D), in SF_6 and Xe solutions, respectively. After accounting for hard sphere geometrical factors, CO J relaxation appears to be ~20% more efficient in SF_6 than Xe similar to the results reported here.[97]

TABLE V. Hard sphere radii (Å).[a]

Reference	N_2O	Xe	SF_6	$d_{N_2O,SF_6}{}^2/d_{N_2O,Xe}{}^2$
HCB[111]	1.95	2.03	2.75	1.39
KD[b,112,113]	1.65	1.98	2.75	1.48
JJ[32]	1.85	1.96	2.63	1.38
RAS[114]	1.91	2.02	2.56	1.29
Average	1.84	2.00	2.67	1.38

[a] $d_{N_2O,SF_6}{}^2 = (r_{N_2O} + r_{SF_6})^2$; $d_{N_2O,Xe}{}^2 = (r_{N_2O} + r_{Xe})^2$.
[b] Kinetic diameters.

As indicated above, the N_2O RER rate given by 2DIR analysis is 1.9 times faster in SF_6 than in Xe in the density regime where IBC model dynamics are observed. Given $k_{rot} \propto \sigma_{AB}\bar{v}_{AB}$, the higher temperature of the SF_6 solutions can account for only ~5% of the increase in the RER rate relative to Xe. The difference in reduced solute–solvent mass results in a ~1% slower rate for SF_6 compared to the very slightly lighter Xe. However, the larger size of SF_6 relative to Xe (Tables I and V) accounts for a more significant contribution to the faster N_2O RER rate in SF_6 in this hard sphere description. Using the averaged hard sphere diameters (Table V), the geometric factor σ_{AB} accounts for ~40% faster RER rate in SF_6 relative to Xe. Thus, taking effects of temperature, mass, and hard sphere diameter into account, the observed N_2O RER cross section is still ~30% more efficient for N_2O in SF_6 than Xe.

The larger rotational energy transfer efficiency resulting from N_2O–SF_6 collisions relative to N_2O–Xe collisions may be attributed to two significant factors. The RER process in Xe at infinite dilution is solely determined by intermolecular N_2O–Xe rotation to translation or translation to rotation (R ↔ T) collisional energy exchange. However, the RER process in SF_6 can proceed through both R ↔ T and R ↔ R processes, or R,T ↔ R′, T′ collisional energy exchange more generally.[13,96,100] The internal rotational energy states of the molecular solvent (SF_6) as compared to the monoatomic (Xe) bath provides a more entropically favorable partner for collisional energy relaxation/transfer at finite temperatures (~300 K) of these solutions. Given that 351 cm^{-1} is the lowest frequency normal mode of SF_6, R ↔ V energy transfer is not expected to play a role in the RER process of interest here. Electronic factors, however, could also play a role in enhancing the rate of rotational energy exchange in SF_6 relative to Xe. In contrast to the atomic Xe collision partner, SF_6 has a hexadecapole moment.[101] This permanent charge distribution contributes to the angular anisotropy of the interaction potential, which is known to be responsible for rotational energy transfer allowing additional torque to be generated upon collisional interactions.[13,25,32] Furthermore, the larger (~12%, Table I) SF_6 polarizability coupling to the relatively weak N_2O dipole (μ = 0.16 D) may also contribute to the enhanced N_2O rotational energy transfer rate in SF_6.

This difference in RER efficiency is reminiscent of differences in RER described for smooth and rough hard sphere model in the early theoretical description of rotational and translational energy transfer in dense fluids resulting from binary collisions resulting from harsh repulsive forces.[102,103] Smooth and rough hard spheres differ in their efficiency to couple translational and rotational motion in binary collisions. Perfectly smooth hard spheres correspond to no coupling.[104,105] For perfectly rough hard spheres, molecules grip each other without slipping during a collision, allowing maximal efficiency in the transfer of rotational angular momentum and rotational energy.[32,33] In this context, SF_6 is closer to the rough hard sphere limit than Xe and hence exhibits a more efficient rotational energy transfer rate.

2. IBC breakdown, three-regime behavior, and the onset of many body effects

Simple IBC breakdown for N_2O RER, signaling the onset of many body effects, occurs at only slightly different densities for SF_6 (~3.4 M) and Xe (~4.2 M) solutions along their respective isotherms

(Figs. 5 and 6). The slightly lower IBC breakdown density in SF_6 relative to Xe is consistent with van der Waals estimates of second virial coefficients (B_2 Table I) or excluded volume considerations for these two fluids. Furthermore, a *Q*-branch-like pure vibrational feature attributed to a hindered rotor N_2O population in the ensemble becomes evident in N_2O ν_3 absorption spectra at ~4M solvent concentration in both Xe and SF_6. This observation is consistent with the onset of many body effects on RER rates and IBC breakdown at the same densities.

The onset of many body effects (~4 M), however, results in qualitatively different RER density dependencies in these two nondipolar, spherical solvents (Figs. 5 and 6). A more traditional "three-regime" density dependence is observed for RER as a function of SF_6 density where a plateau region well below the solvent's critical density is observed. However, the N_2O RER rates in Xe along a near critical isotherm increase more rapidly than linear density dependence would predict, consistent with a detectable contribution of many body effects to the energy fluctuation dynamics of the free rotors in the ensemble. The RER rate continues to dramatically increase as the Xe critical point is approached at 8.4 M (Fig. 6). In contrast, N_2O RER rates in SF_6 *decrease* relative to the linear density dependence of the lower concentration state points where many body effects appear to contribute to the solvation of this solution. The RER rates are *slower* than the IBC extrapolated values for reduced densities in the range of $\sim 0.8 \leq \rho_c \leq \sim 1.4$ or for SF_6 concentrations from ~4 to ~7 M for this near critical isotherm, $T^* = 1.01$. Beyond ~7M SF_6 (or $\rho^* = \sim 1.5$), the RER rate exceeds the IBC extrapolated values consistent with multiple collisions enhancing rotational energy transfer for the rotor population, as found for the Xe density trends when IBC breakdown occurs. Although preliminary evidence for a plateau in the density dependence of the N_2O RER in SF_6 indicative of the onset of long-time fluctuations near the critical point has been reported earlier,[12] the additional higher density state points at 5.79 M ($\rho^* = 1.17$) and 7.70 M ($\rho^* = 1.51$) provide additional accuracy to this 2DIR detected phenomenon, underscoring the qualitatively different solvent density dependence in Xe and SF_6.

The key solvent property that distinguishes these two solvation effects at densities when many body effects become important is the proximity to the critical region for these isotherms. For SF_6 solutions, IBC breakdown initially occurs at a density close to the critical point ($\rho^* = \sim 0.8$, ~4 M); in Xe, many body effects are evident at about the same absolute density as for SF_6 (~4 M); however, this concentration (~4 M) is further from the critical density ($\rho^* = \sim 0.5$) of Xe. Hence, the effects of long-range spatial correlations that characterize supercritical fluids for temperature near T_c will have a significantly smaller impact on N_2O solvation in Xe when many body effects just start to be important. In contrast, the 2DIR derived fluctuation rates suggest that for the free rotor N_2O population in SF_6, at the near critical density where IBC breakdown is occurring and many body effects are evident, there is coupling of the local solvation environment to the critical fluctuation dynamics of the solvent resulting from the developing long-range spatial correlations. This effect appears at $\rho^* = \sim 0.8$ in SF_6 and is centered near $\rho^* \sim 1$ where such density fluctuation correlations are maximal and the fluctuation timescale is the slowest.[64,65,106] Such coupling between the longer length scale critical fluid dynamics and local solvation, here RER collision dynamics, have been described in previous MD simulation studies,[63,67,107] and they can account for the critical slowing observed here directly in the 2DIR direct measure of fluctuation dynamics in the N_2O local solvation environment.

In contrast, this coupling is not effective in Xe solutions. As noted above, many body effects on the N_2O RER dynamics in Xe are evident at approximately the same absolute number density as for SF_6 solutions; but, this corresponds to a lower Xe reduced density. Thus, as the Xe solvent density approaches that of the critical region, say $\rho^* \sim 0.8$, where critical slowing effects are evident for SF_6; these additional many body interactions appear to provide a shielding effect from the longer range density correlations for N_2O in Xe solutions as they couple to the local N_2O RER collision mechanism. As a consequence of this proposed shielding effect, the three-density regime behavior, i.e., a plateau in RER rates, is not observed for these Xe solutions at least as measured by the 2DIR energy fluctuation dynamics of the N_2O free rotor population. Finally, as shown previously,[12] the 2DIR determined *J*-scrambling rates can be used to identify separate quasi-free rotor (gas) and hindered rotor contributions to the observed N_2O ν_3 absorption spectrum at each solvent density.

B. Vibrational energy relaxation

The solvent and density dependence of the vibrational energy relaxation of the N_2O ν_3 fundamental can be contrasted with that of the corresponding 2DIR determined RER rates. Only the dispersed magic angle pump–probe response on the blue side of the ν_3 GSB-SE signal is used to determine the VER kinetics reported here. In the dense gas and SCF solutions, the pump–probe response in this spectral region is dominated by N_2O molecules in the more gas-like solvent environments, allowing for comparison with the sample ensemble population giving rise to the RER dynamics (Figs. 1 and S1). As shown previously, one-color, magic angle pump–probe responses resonant with the N_2O $\nu_3 = 1$ vibrational level (0 0 1) exhibit a bi-exponential decay in the gas, SCF, and liquid SF_6 phase solutions studied[12] [(n_1 n_2 n_3) corresponds to n_1 quanta in the ν_1 mode etc.]. The observed density dependent pump–probe responses were well-fit by a two-step kinetic model corresponding to the initial collision induced N_2O intramolecular decay from the pump-excited asymmetric ν_3 to the symmetric ν_1 stretching mode, (0 0 1) → (1 0 0), and a second much slower decay component due to the relaxation of the subsequently populated intermediate N_2O ν_1 level to the ground state, (1 0 0) → (0 0 0), via solvent collisions. The bi-exponential fit (red) and the two components (blue and green) contributing to this VER model are illustrated in Figs. 7(a) and 7(b) for N_2O in two representative SF_6 solvent densities ($\rho^* = 0.16$, 0.81 M and $\rho^* = 1.51$, 7.7 M). The faster relaxation of the initial decay component (blue) is attributed to the resonance of the N_2O ν_3–ν_1 energy gap (~940 cm^{-1}) and the highest frequency SF_6 fundamental, an asymmetric stretching mode at 948 cm^{-1}, enabling a resonant V → V solute–solvent collisional energy transfer process. Lacking a single SF_6 vibrational mode matching the (1 0 0) → (0 0 0) energy gap, relaxation from the N_2O (1 0 0) symmetric ν_1 level to the ground state is governed by a higher order process; hence, the VER rate for this ν_1 component is consistent with the experimentally determined ~30–40 times slower second decay in the observed pump–probe response (green).[12] Since quantitative measures of this slower decay were beyond the current dynamic range of our experimental setup, only the rates associated

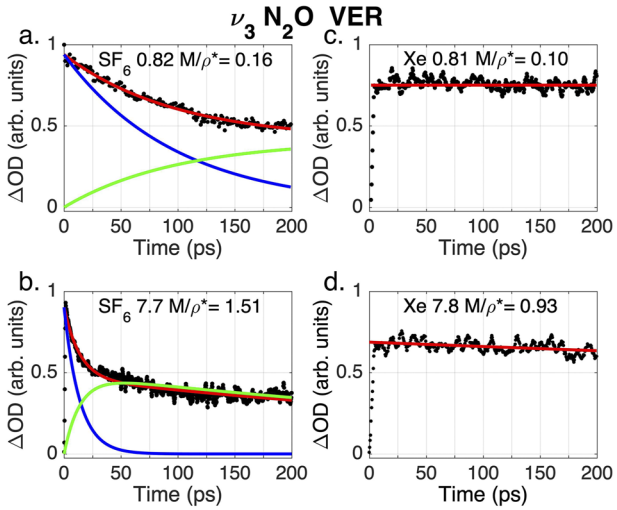

FIG. 7. Representative one-color magic angle pump–probe spectra of the N_2O ν_3 asymmetric stretch mode in near critical density for (a) SF_6 at $\rho^* = 0.16$, 0.82 M, (b) SF_6 at $\rho^* = 1.51$, 7.7 M, (c) Xe at $\rho^* = 0.10$, 0.81 M, and (d) Xe at $\rho^* = 0.93$, 7.8M. The two best-fit determined contributions (in blue and green) to the bi-exponential total decay (red) are shown for the SF_6 solutions. In contrast, in Xe solutions, only a slight decay (~5%) is observed on a 200 ps timescale for the highest density solution (d). The two-component kinetic fit plotted in (b) has been described previously.[1] The ν_3 $v = 1$ lifetime is ~300 times slower in Xe than SF_6.

with the faster VER component will be considered here. However, after excitation of the N_2O ν_3 rovibrational band in SF_6, *rotational* equilibrium is re-established on the timescale of picoseconds and full *vibrational* relaxation is complete on the timescale of nanoseconds.[12]

1. N_2O ν_3 VER in SF_6

The best-fit determined initial decay rates ($1/T_1$) of the N_2O ν_3 (0 0 1) level are plotted as a function of SF_6 density in Fig. 8. ν_3 vibrational lifetimes from 108 to 6.1 ps are observed across the studied SF_6 density range (Table III). Analogous to the 2DIR results, N_2O ν_3 pump–probe measurements at two additional SF_6 state points in the near critical region at 5.79 M ($\rho^* = 1.13$) and 7.7 M ($\rho^* = 1.51$) were carried out here in addition to the previously reported SF_6 state points in order to also better define the VER dynamics in the SCF region.[12] Note the corresponding N_2O vibrational population decay in the SF_6 liquid, $\rho^* = 1.87$, 9.78 M (T = 293 K), is also included in this figure. The red dashed line in Fig. 8 is the best fit of a simple density dependent IBC model to the lowest gas phase SF_6 densities for this near critical isotherm. This VER treatment is analogous to that shown for RER results in Fig. 5. The corresponding rate constant (k_{VER}) for this initial N_2O VER in SF_6 (slope of red dashed line) is 2.6×10^{-11} cm^3 s^{-1} molecule^{-1} in the lower density region. k_{VER} is thus a factor of ~7 smaller than the corresponding RER rate constant k_{RER} in the density regime where IBC kinetics are observed (Table III). The resonant V → V solute–solvent energy transfer mechanism accounting for the faster initial decay component results in a N_2O ν_3 vibrational lifetime corresponding to ~12 N_2O–SF_6 collisions as compared to the 1.7 collisions required for re-establishing rotational equilibrium.

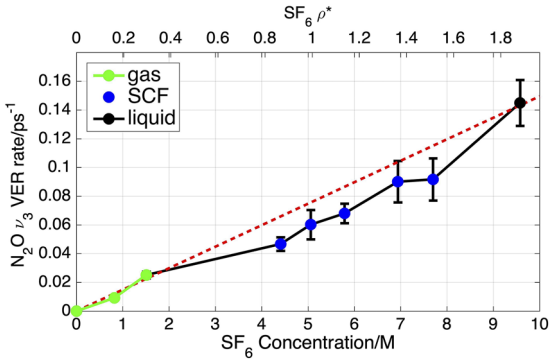

FIG. 8. VER rate of the N_2O ν_3 mode ($1/T_1$) corresponding to the initial pump–probe decay as a function of SF_6 concentration (M) and ρ^*. The dashed red line is the linear best fit to the lowest density state points and represent the predicted rates of VER resulting from a simple IBC model.

Even for the more limited precision of the VER rates, owing to the 200 ps range of our current 2DIR focused experimental system and the bi-exponential pump–probe decay character, the N_2O ν_3 VER density dependence in SF_6 differs qualitatively from that found for the 2DIR determined RER rates (Fig. 5), apart from the quantitatively slower VER timescale. The rate of VER slightly decreases below the simple IBC predicted rates as seen for RER processes for densities where many body effects become evident in SF_6 (~3.4 M). However, as the solvent density increases from $\rho^* = 0.86$ (4.41 M) to $\rho^* = 1.51$ (7.70 M), VER rates exhibit a nearly linear density dependence in this SCF density regime. The observed VER density dependence contrasts to the slowing and then enhanced rates seen for RER at the same SF_6 densities (Fig. 5). The different RER and VER density dependence in the region where many body effects appear may be attributable to the longer timescale and different collisional mechanisms, R ↔ T vs resonant V ↔ V, controlling the relaxation of these different internal degrees of freedom. Thus, the role of local critical slowing effects resulting from the long correlation length scale density fluctuations characteristic of compressible SCFs in near critical regions is less evident for VER than for RER in this solute–solvent system. Furthermore, the N_2O ν_3 VER rate in SF_6 liquid (Fig. 8) is relatively well captured by an IBC model density dependence over the dilute gas to liquid density range. Inclusion of the radial pair distribution into the VER rate expression, as carried out for VER in other dense gas, near critical, and supercritical solution studies,[29,49,52,53,55] may provide better quantitative agreement between the IBC modeled and observed VER rate density dependence for this solution system. However, the main conclusions to be drawn here are that N_2O VER and RER have a different density dependence in SF_6 solutions and the critical density fluctuations are less effectively coupled to the local solvation dynamics relevant for the relaxation of vibrational energy than for RER of N_2O ν_3 in supercritical SF_6 along this $T^* = 1.01$ isotherm.

In a previous set of pump–probe measurements of the T_{1u} asymmetric CO stretching mode of $W(CO)_6$ in C_2H_6, CO_2, and CHF_3 as a function of solvent density for a near critical isotherm, characteristic three-regime behavior with a plateau in the $\rho^* = 0.8$–1.2 region was observed.[39] Although this near critical

behavior phenomenologically resembles a critical slowing effect for T_1, the density independence around $\rho^* \sim 1$ was attributed to a cancellation of structural and thermodynamic quantities in the near critical regime and not *explicitly* on dynamic factors, or enhanced local solvent clustering, at these state points.[39,44,50,51] In contrast, the 2DIR analysis directly reports on fluctuation timescales and the plateau region for N_2O RER in SF_6 (Fig. 6) is attributable to the local solvation coupling to the solvent's critical slowing fluctuations. Although three-regime density dependence is not observed for N_2O VER in SF_6, the apparent lack of coupling of this VER process to the same explicit critical dynamics effects in SF_6 evident for RER is at least in formal agreement with the VER description given for $W(CO)_6$ in that solvation fluctuation timescales are not directly evident from the VER density dependence. In other vibrational lifetime studies of near critical water solutions, a modified IBC model description was found to match the observed temperature and density dependent T_1 measurements. However, no near critical ($T^* \sim 1.01$) isotherms were examined in these previous studies and three-regime behavior, as found for the $W(CO)_6$ lifetime,[39] was not observed.[52,53,55]

2. N_2O ν_3 VER in Xe

Analogous dispersed, magic angle pump–probe measurements of the N_2O ν_3 VER kinetics in Xe solutions with solvent densities ranging from $\rho^* = 0.10$ (0.81 M) to 0.93 (7.8 M) along the near critical $T^* = 1.005$ isotherm were obtained. The goal was to contrast these responses with the corresponding VER dynamics in SF_6 solutions and with the N_2O RER in Xe and SF_6. In striking contrast to the pump–probe decays in SF_6 solutions [Figs. 7(a) and 7(b)], no significant N_2O ν_3 vibrational population decay is observed in these Xe solutions up to the longest delay times measured (200 ps) as shown for N_2O pump–probe responses in $\rho^* = 0.10$ (0.81 M) and $\rho^* = 0.93$ (7.8 M) Xe solutions [Figs. 7(c) and 7(d)]. This figure highlights the drastically different VER times in these two solvents.

Given the prior explanation of the N_2O ν_3 VER process in SF_6,[12] this result is not surprising. In the absence of any vibrationally resonant or nonresonant V → V (or V → R) energy transfer mechanism possible in the Xe solvent, only V → T processes can account for VER of infinitely dilute N_2O in Xe solutions. Thus, the very slow pump–probe decays in Xe solutions is consistent with the proposed resonant V → V mechanism for N_2O ν_3 VER in SF_6. V → T energy transfer is much less efficient than resonant V → V processes[25] and this can be readily understood by Fermi golden rule considerations. Only in the highest Xe concentration observed in this current study, 7.8M ($\rho^* = 0.93$), is a small pump–probe decay resulting in ~5% ΔOD reduction after 200 ps observed [Fig. 7(d)]. This corresponds to an estimated ν_3 vibrational lifetime of ~2.5 ns or initial VER rate constant $k_{VER} \sim 8.5 \times 10^{-14}$ cm^3 s^{-1} molecule^{-1} at this Xe density. Hence, the N_2O ν_3 lifetime is ~300 times slower in Xe relative to SF_6 at comparable densities (Table III). These dramatically different VER relaxation results in SF_6 and Xe illustrate how much more sensitively dependent VER is on the quantum structure of the solute–solvent system relative to RER. In particular, the resonant vibrational gaps offered by the internal degrees of freedom of SF_6 accelerate the loss of energy in the optically prepared excited state by several orders of magnitude relative to V → T mechanisms alone in Xe. Furthermore, given this T_1 (2.5 ns) estimate and the 2DIR determined CLS decay at this same Xe density ($\tau_c = 0.8$ ps, Table II), rotational equilibrium is established at least ~3000 times more rapidly than vibrational equilibrium for N_2O in Xe at this near critical state point.

V. CONCLUSIONS

These experimental results demonstrate how ultrafast 2DIR spectroscopy can be an effective technique for learning about rotational energy transfer in solutions from the low-density regime, where IBC dynamics are evident, through the critical region where the dynamical effects resulting from the long-range density correlations are found and at even higher SCF densities where many body effects dominate. Although a simple IBC model description is sufficient up to solvent densities of ~4M for the systems studied here, the RER dynamics of N_2O in two similar non-dipolar solvents, Xe and SF_6, show very different concentration dependence as the critical density is approached. The slower density fluctuations accompanying the longer length scale density correlations couple to the local N_2O free rotor environments and result in slower rotational energy transfer rates in SF_6 at a density near the critical density ($\rho^* \sim 0.8$). Many body effects, e.g., IBC breakdown and a distinct *Q*-branch-like feature in the FTIR spectrum, also appear in N_2O solutions at this same ~4 M SF_6 solvent density. Although the same many body effects are evident at approximately the same number density (~4 M) in Xe, this density is much further from the critical point and many body interactions appear to shield the N_2O rotors from coupling to the long correlation length fluctuations. 2DIR studies of N_2O ν_3 RER as a function of SF_6 density at higher temperatures, $T > 1.1T^*$, will be carried out to test the critical fluctuation coupling hypothesis described here. Long-scale density fluctuations diminish in importance at these higher temperatures.[39,64–66]

The effects of critical slowing on RER might be expected to be evident for N_2O in near critical solutions of carbon tetrachloride ($\rho_c = 3.62$ M), propane ($\rho_c = 5.1$ M), and dichlorodifluoromethane ($\rho_c = 4.67$ M), where the critical density, like that of SF_6 ($\rho_c = 5.1$ M), is relatively low and close to the solvent concentration where many body effects begin to be evident for N_2O in SF_6 and Xe solutions. In contrast, no critical slowing effects would be expected for N_2O RER in near critical CO_2 solutions where the critical density (10.63 M) is even greater than that of Xe and, thus, shielding effects are expected to dominate given the mismatch in density anticipated for where IBC breakdown will occur and ρ_c for CO_2.

While spectral shifts and line broadening effects consistent with local density augmentation in near critical solutions have been observed, such measurements do not reveal direct dynamical information. To our knowledge, these 2DIR based results are the first *direct* experimental measures showing the influence of the critical point fluctuations, arising from the special *long-range* spatial correlations at near critical state points, to manifest dynamics, here RER, on a *local,* i.e., molecular, length scale. Vibrational peak shifts, a widely observed and analyzed spectroscopic measure of solvation effects in the critical point region, do not show the solvent specific effects of critical slowing in SF_6 and Xe solutions as this report demonstrates and this further serves to highlight the potential power that 2DIR can bring to the study of critical properties in solutions.

N_2O RER is a highly efficient process. Following ν_3 asymmetric stretching, excitation of rotational equilibrium is re-established after 1.7 and 2.4 collisions in SF_6 and Xe, respectively, in the IBC

density region and highlights the precision of the 2DIR technique for quantitating rotational dynamics in dense media. The ~30% higher efficiency in SF_6 is attributed to the additional R, T ↔ R′, T′ pathways available for the molecular collision partner. However, electronic factors, such as the SF_6 hexadecapole moment or the larger SF_6 polarizability (Table I) coupling to the weak N_2O dipole, can be contributing factors as well. The relation to classical rough/smooth hard sphere models describing the exchange of rotational and translation momentum and energy was noted, and ongoing MD simulations will be used to further address the origins of this Xe, SF_6 efficiency difference.

The density dependence of N_2O VER is also strikingly different in Xe and SF_6, and it underscores that VER has a highly variable rate due to the inherently quantum nature ($\hbar\omega_{vib} > kT$) of this relaxation mechanism. The N_2O ν_3 lifetime is ~300 times shorter in SF_6 than in Xe because the internal degrees of freedom for the molecular solvent have a resonant V → V relaxation pathway allowing relatively efficient VER in SF_6. Of course, no such mechanism is possible in the inert gas solvent. Furthermore, the VER density dependence in SF_6 in the SCF region does not resemble that for RER over the corresponding range. The longer VER timescale, k_{RER}, is nearly an order of magnitude greater than k_{VER} for the initial VER component, and the different character of the solute–solvent interaction required for rotational and vibrational relaxation, i.e., collisions and many body effects capable of changing angular kinetic energy as compared to accepting vibrational energy, will contribute to the observed different VER and RER density dependence in SF_6. Thus, these data show that universal scaling behavior in infinitely dilute critical solutions may not be relevant for all energy transfer processes.

Finally, the 2DIR and pump–probe results demonstrate that rotational and vibrational equilibria are established on very different timescales even in liquid-like solvent/bath densities at least for small molecular systems. While only 1.5/2.5 collisions are needed for N_2O rotations to thermalize in SF_6/Xe, N_2O vibrational relaxation may take hundreds of collisions or more to return the molecule fully to thermal equilibrium.

In a subsequent paper, we will report on MD simulation studies of the absorption and rotational and vibration energy relaxation processes corresponding to these N_2O in SF_6 and Xe solutions at the experimental state points described here. These ongoing simulations are intended to provide additional evidence supporting the proposed mechanisms for the density dependent dynamics uncovered by these 2DIR and pump–probe measurements. In particular, we will look for these computational studies to provide additional insight for understanding the near critical solvation effects both in terms of the timescale of the solvent critical fluctuation dynamics coupling to the solute environment and the local density enhancement description. Continuing to extend these 2DIR measurements to other dense fluids for the same "reporter," i.e., solute, as well as different "reporters" in the same environments will help provide a quantitative test for the generality of these results and uncover additional factors controlling rovibrational dynamics and near critical solvation effects in dense fluids.

Aside from higher temperature 2DIR studies of N_2O in SF_6 and in more near critical point densities of Xe, N_2O 2DIR spectra in other accessible critical fluids will be observed for comparison with these two solvents. Future experimental studies will be required to carry out 2DIR/pump–probe measurements of an alternative solute reporter molecule (e.g., CO_2, HCl) in the same Xe and SF_6 dense solvent baths testing the effects of dipole and quadrupole interactions and larger, rotational energy spacings of the solute.

SUPPLEMENTARY MATERIAL

See the supplementary material for the following: FTIR analysis of the N_2O ν_3 band in SF_6, comparison of N_2O ν_3 FTIR results in SF_6 and Xe, expanded view of N_2O ν_3 vibrational absorption feature in the 4.4 M ($\rho^* = 0.86$) SF_6 solution spectrum, and 2DIR spectra and resulting CLS decays of N_2O ν_3 in Xe and SF_6 at all solvent densities studied.

ACKNOWLEDGMENTS

The authors gratefully acknowledge the support provided by the National Science Foundation Grant No. CHE-2102427 (L.D.Z.) and the Boston University Photonics Center. We also acknowledge useful discussions with Kai Töpfer and Markus Meuwly (University of Basel) regarding relaxation dynamics in these systems.

AUTHOR DECLARATIONS

Conflict of Interest

The authors have no conflicts to disclose.

Author Contributions

Matthew C. Rotondaro: Data curation (lead); Formal analysis (lead); Methodology (lead); Writing – original draft (lead). **Arkash Jain**: Data curation (supporting); Formal analysis (supporting); Methodology (supporting); Validation (supporting). **Shyamsunder Erramilli**: Supervision (supporting); Writing – review & editing (supporting). **Lawrence D. Ziegler**: Conceptualization (lead); Funding acquisition (lead); Project administration (lead); Supervision (lead); Writing – review & editing (lead).

DATA AVAILABILITY

The data that support the findings of this study are available within the article and its supplementary material.

REFERENCES

[1] J. Foster and R. S. Miller, in *High Pressure Processes in Chemical Engineering*, edited by M. Lackner (ProcessEng Engineering GmbH, 2010), pp. 53–75.

[2] C. Guardiola, P. Olmeda, B. Pla, and P. Bares, "In-cylinder pressure based model for exhaust temperature estimation in internal combustion engines," Appl. Therm. Eng. **115**, 212–220 (2017).

[3] P. V. Farrell and B. D. Peters, "Droplet vaporization in supercritical pressure environments," Acta Astronaut. **13**, 673–680 (1986).

[4] O. Kajimoto, "Solvation in supercritical fluids: Its effects on energy transfer and chemical reactions," Chem. Rev. **99**, 355–390 (1999).

[5] Ž. Knez, E. Markočič, M. Leitgeb, M. Primožič, M. Knez Hrnčič, and M. Škerget, "Industrial applications of supercritical fluids: A review," Energy **77**, 235–243 (2014).

[6]G. Brunner, "Applications of supercritical fluids," Annu. Rev. Chem. Biomol. Eng. **1**, 321–342 (2010).
[7]M. K. Hrnčič, D. Cör, M. T. Verboten, and Ž. Knez, "Application of supercritical and subcritical fluids in food processing," Food Qual. Saf. **2**, 59–67 (2018).
[8]M. Perrut, "Supercritical fluid applications: Industrial developments and economic issues," Ind. Eng. Chem. Res. **39**, 4531–4535 (2000).
[9]P. B. Deshpande, G. A. Kumar, A. R. Kumar, G. V. Shavi, A. Karthik, M. S. Reddy, and N. Udupa, "Supercritical fluid technology: Concepts and pharmaceutical applications," PDA J. Pharm. Sci. Technol. **65**, 333 (2011).
[10]H. Machida, M. Takesue, and R. L. Smith, "Green chemical processes with supercritical fluids: Properties, materials, separations and energy," J. Supercrit. Fluids **60**, 2–15 (2011).
[11]A. Mandal, G. Ng Pack, P. P. Shah, S. Erramilli, and L. D. Ziegler, "Ultrafast two-dimensional infrared spectroscopy of a quasifree rotor: *J* scrambling and perfectly anticorrelated cross peaks," Phys. Rev. Lett. **120**, 103401 (2018).
[12]G. Ng Pack, M. C. Rotondaro, P. P. Shah, A. Mandal, S. Erramilli, and L. D. Ziegler, "Two-dimensional infrared spectroscopy from the gas to liquid phase: Density dependent *J*-scrambling, vibrational relaxation, and the onset of liquid character," Phys. Chem. Chem. Phys. **21**, 21249–21261 (2019).
[13]A. Schiffman and D. W. Chandler, "Experimental measurements of state resolved, rotationally inelastic energy transfer," Int. Rev. Phys. Chem. **14**, 371–420 (1995).
[14]P. Warneck, *Chemistry of the Natural Atmosphere* (Academic Press, London, 2000).
[15]E. Weitz and G. Flynn, "Laser studies of vibrational and rotational relaxation in small molecules," Annu. Rev. Phys. Chem. **25**, 275–315 (1974).
[16]J. Foster and R. S. Miller, in *High Pressure Processes in Chemical Engineering*, edited by M.Lackner (ProcessENG Engeneering GmbH, 2010), pp. 53–75.
[17]P. K. Cheo and R. L. Abrams, "Rotational relaxation rate of CO_2 laser levels," Appl. Phys. Lett. **14**, 47–49 (1969).
[18]M. L. Unland and W. H. Flygare, "Direct measurement of rotational relaxation," J. Chem. Phys. **45**, 2421–2432 (1966).
[19]R. G. Gordon, W. Klemperer, and J. I. Steinfeld, "Vibrational and rotational relaxation," Annu. Rev. Phys. Chem. **19**, 215–250 (1968).
[20]D. V. Kalinin, D. K. Bronnikov, Y. G. Selivanov, T. Gabard, J.-P. Champion, and J.-C. Hilico, "Measurement of rotational relaxation in the ground state of methane perturbed by argon at low temperature," J. Quant. Spectrosc. Radiat. Transfer **62**, 13–27 (1999).
[21]E. H. Carnevale, C. Carey, and G. Larson, "Ultrasonic determination of rotational collision numbers and vibrational relaxation times of polyatomic gases at high temperatures," J. Chem. Phys. **47**, 2829–2835 (1967).
[22]M. L. Strekalov, "Determination of the rotational relaxation cross section of carbon dioxide from spectral measurements," Opt. Spectrosc. **98**, 1–5 (2005).
[23]P. R. Dahoo, D. Jasmin, P. Brosset, B. Gauthier-Roy, and L. Abouaf-Marguin, "Vibrational relaxation study of O_3 in rare gas and nitrogen matrices by time resolved infrared–infrared double resonance spectroscopy," J. Chem. Phys. **108**, 8541–8549 (1998).
[24]D. A. V. Kliner and R. L. Farrow, "Measurements of ground-state OH rotational energy-transfer rates," J. Chem. Phys. **110**, 412–422 (1998).
[25]J. T. Yardley, *Introduction to Molecular Energy Transfer* (Academic Press, New York, 1980).
[26]R. Holmes, G. R. Jones, and R. Lawrence, "Rotational relaxation in carbon dioxide and nitrous oxide," J. Chem. Phys. **41**, 2955–2956 (1964).
[27]R. Holmes, G. R. Jones, and N. Pusat, "Combined viscothermal and thermal relaxation in polyatomic gases," Trans. Faraday Soc. **60**, 1220–1229 (1964).
[28]R. J. Gallagher and J. B. Fenn, "Relaxation rates from time of flight analysis of molecular beams," J. Chem. Phys. **60**, 3487–3491 (1974).
[29]R. J. Finney, M. Wolfe, and J. Jonas, "NMR study of angular momentum relaxation in fluids. I. Compressed CF_4," J. Chem. Phys. **67**, 4004–4011 (1977).
[30]J. H. Campbell, S. J. Seymour, and J. Jonas, "Reorientational and angular momentum correlation times in gaseous tetrafluoromethane at moderate densities," J. Chem. Phys. **59**, 4151–4156 (1973).
[31]C. J. Jameson and A. K. Jameson, "Effective collision cross sections for SF_6 from nuclear magnetic relaxation," J. Chem. Phys. **88**, 7448–7452 (1988).
[32]C. J. Jameson and A. K. Jameson, "Angular momentum relaxation in binary collisions. Comparison of cross sections," J. Chem. Phys. **93**, 3237–3244 (1990).
[33]J. DeZwaan and J. Jonas, "Density and temperature effects on motional dynamics of SF_6 in the supercritical dense fluid region," J. Chem. Phys. **63**, 4606–4612 (1975).
[34]S. C. Tucker, "Solvent density inhomogeneities in supercritical fluids," Chem. Rev. **99**, 391–418 (1999).
[35]M. J. Clouter, H. Kiefte, and N. Ali, "Anomalous behavior in the vibrational Raman spectrum of oxygen under near-critical conditions," Phys. Rev. Lett. **40**, 1170–1173 (1978).
[36]Y. P. Sun, M. A. Fox, and K. P. Johnston, "Spectroscopic studies of p-(N, N-dimethylamino)benzonitrile and ethyl p-(N,N-dimethylamino)benzoate in supercritical trifluoromethane, carbon dioxide, and ethane," J. Am. Chem. Soc. **114**, 1187–1194 (1992).
[37]D. Ben-Amotz, F. LaPlant, D. Shea, J. Gardecki, and D. List, "Supercritical fluid technology," ACS Symp. Ser. **488**, 18–30 (1992).
[38]S. Akimoto and O. Kajimoto, "Solvent-induced shift of the Raman spectra in supercritical fluids," Chem. Phys. Lett. **209**, 263–268 (1993).
[39]R. S. Urdahl, D. J. Myers, K. D. Rector, P. H. Davis, B. J. Cherayil, and M. D. Fayer, "Vibrational lifetimes and vibrational line positions in polyatomic supercritical fluids near the critical point," J. Chem. Phys. **107**, 3747–3757 (1997).
[40]H. Nakayama, K.-i. Saitow, M. Sakashita, K. Ishii, and K. Nishikawa, "Raman spectral changes of neat CO_2 across the ridge of density fluctuation in supercritical region," Chem. Phys. Lett. **320**, 323–327 (2000).
[41]M. I. Cabaço, M. Besnard, T. Tassaing, and Y. Danten, "Vibrational and rotational relaxation of hexafluorobenzene studied by Raman scattering in the supercritical domain," J. Mol. Liq. **125**, 100–106 (2006).
[42]K.-i. Saitow, K. Otake, H. Nakayama, K. Ishii, and K. Nishikawa, "Local density enhancement in neat supercritical fluid due to attractive intermolecular interactions," Chem. Phys. Lett. **368**, 209–214 (2003).
[43]T. Tassaing, R. Oparin, Y. Danten, and M. Besnard, "Water–CO_2 interaction in supercritical CO_2 as studied by infrared spectroscopy and vibrational frequency shift calculations," J. Supercrit. Fluids **33**, 85–92 (2005).
[44]D. J. Myers, M. Shigeiwa, M. D. Fayer, and B. J. Cherayil, "Vibrational lifetimes and spectral shifts in supercritical fluids as a function of density: Experiments and theory," J. Phys. Chem. B **104**, 2402–2414 (2000).
[45]S. A. Egorov and J. L. Skinner, "Vibrational line shifts in supercritical fluids," J. Phys. Chem. A **104**, 483–489 (2000).
[46]L. E. Bowman, B. J. Palmer, B. C. Garrett, J. L. Fulton, C. R. Yonker, D. M. Pfund, and S. L. Wallen, "Infrared and molecular dynamics study of D_2O rotational relaxation in supercritical CO_2 and Xe," J. Phys. Chem. **100**, 18327–18334 (1996).
[47]N. Wada, M. Saito, D. Kitada, R. L. Smith, H. Inomata, K. Arai, and S. Saito, "Local excess density about substituted benzene compounds in supercritical CO_2 based on FT-IR spectroscopy," J. Phys. Chem. B **101**, 10918–10922 (1997).
[48]S. M. Howdle and V. N. Bagratashvili, "The effects of fluid density on the rotational Raman spectrum of hydrogen dissolved in supercritical carbon dioxide," Chem. Phys. Lett. **214**, 215–219 (1993).
[49]D. Schwarzer, J. Troe, and M. Zerezke, "The role of local density in the collisional deactivation of vibrationally highly excited azulene in supercritical fluids," J. Chem. Phys. **107**, 8380–8390 (1997).
[50]B. J. Cherayil and M. D. Fayer, "Vibrational relaxation in supercritical fluids near the critical point," J. Chem. Phys. **107**, 7642–7650 (1997).
[51]D. J. Myers, M. Shigeiwa, M. D. Fayer, and B. J. Cherayil, "Density dependent vibrational relaxation in supercritical fluids," Chem. Phys. Lett. **313**, 592–599 (1999).
[52]D. Schwarzer, J. Lindner, and P. Vöhringer, "OH-stretch vibrational relaxation of HOD in liquid to supercritical D_2O," J. Phys. Chem. A **110**, 2858–2867 (2006).
[53]M. Olschewski, S. Knop, J. Lindner, and P. Vöhringer, "Vibrational relaxation of azide ions in liquid-to-supercritical water," J. Chem. Phys. **134**, 214504 (2011).
[54]D. Czurlok, M. von Domaros, M. Thomas, J. Gleim, J. Lindner, B. Kirchner, and P. Vöhringer, "Femtosecond 2DIR spectroscopy of the nitrile stretching vibration of thiocyanate anions in liquid-to-supercritical heavy water. Spectral diffusion and libration-induced hydrogen-bond dynamics," Phys. Chem. Chem. Phys. **17**, 29776–29785 (2015).

[55] J. Gleim, J. Lindner, and P. Vöhringer, "Vibrational relaxation of carbon dioxide in water," J. Chem. Phys. **156**, 094505 (2022).
[56] M. P. Heitz and M. Maroncelli, "Rotation of aromatic solutes in supercritical CO_2: Are rotation times anomalously slow in the near critical regime?," J. Phys. Chem. A **101**, 5852–5868 (1997).
[57] A. Das, R. Biswas, and J. Chakrabarti, "Dipolar solute rotation in a supercritical polar fluid," J. Phys. Chem. A **115**, 973–978 (2011).
[58] M. P. Heitz and F. V. Bright, "Probing the scale of local density augmentation in supercritical fluids: A picosecond rotational reorientation study," J. Phys. Chem. **100**, 6889–6897 (1996).
[59] C. A. Eckert, B. L. Knutson, and P. G. Debenedetti, "Supercritical fluids as solvents for chemical and materials processing," Nature **383**, 313 (1996).
[60] C. Carlier and T. W. Randolph, "Dense-gas solvent-solute clusters at near-infinite dilution: EPR spectroscopic evidence," AIChE J. **39**, 876–884 (1993).
[61] R. Biswas, J. E. Lewis, and M. Maroncelli, "Electronic spectral shifts, reorganization energies, and local density augmentation of Coumarin 153 in supercritical solvents," Chem. Phys. Lett. **310**, 485–494 (1999).
[62] W. Song and M. Maroncelli, "Local density augmentation in neat supercritical fluids: The role of electrostatic interactions," Chem. Phys. Lett. **378**, 410–419 (2003).
[63] S. C. Tucker and M. W. Maddox, "The effect of solvent density inhomogeneities on solute dynamics in supercritical fluids: A theoretical perspective," J. Phys. Chem. B **102**, 2437–2453 (1998).
[64] K.-i. Saitow, H. Ochiai, T. Kato, and K. Nishikawa, "Correlation time of density fluctuation for supercritical ethylene studied by dynamic light scattering," J. Chem. Phys. **116**, 4985–4992 (2002).
[65] K.-i. Saitow, D. Kajiya, and K. Nishikawa, "Time evolution of density fluctuation in supercritical region. I. Non-hydrogen-bonded fluids studied by dynamic light scattering," J. Phys. Chem. A **109**, 83–91 (2005).
[66] K. Nishikawa and T. Morita, "Inhomogeneity of molecular distribution in supercritical fluids," Chem. Phys. Lett. **316**, 238–242 (2000).
[67] G. Goodyear and S. C. Tucker, "Glass-like behavior in supercritical fluids: The effect of critical slowing down on solute dynamics," J. Chem. Phys. **111**, 9673–9677 (1999).
[68] G. Goodyear, M. W. Maddox, and S. C. Tucker, "The correlation between local and long-range structure in compressible supercritical fluids," J. Chem. Phys. **112**, 10327–10339 (2000).
[69] L. Chieffo, J. J. Amsden, J. Shattuck, M. K. Hong, L. Ziegler, and S. Erramilli, "Vibrational infrared lifetime of the anesthetic nitrous oxide gas in solution," Biophys. Rev. Lett. **01**, 309–316 (2006).
[70] L. R. Chieffo, J. T. Shattuck, E. Pinnick, J. J. Amsden, M. K. Hong, F. Wang, S. Erramilli, and L. D. Ziegler, "Nitrous oxide vibrational energy relaxation is a probe of interfacial water in lipid bilayers," J. Phys. Chem. B **112**, 12776–12782 (2008).
[71] A. N. Hayhurst and A. D. Lawrence, "Emissions of nitrous oxide from combustion sources," Prog. Energy Combust. Sci. **18**, 529–552 (1992).
[72] L. J. Muzio, T. A. Montgomery, G. S. Samuelsen, J. C. Kramlich, R. K. Lyon, and A. Kokkinos, "Formation and measurement of N_2O in combustion systems," Symp. (Int.) Combust. **23**, 245–250 (1991).
[73] A. Colorado, V. McDonell, and S. Samuelsen, "Direct emissions of nitrous oxide from combustion of gaseous fuels," Int. J. Hydrogen Energy **42**, 711–719 (2017).
[74] K. C. Gronborg, S. M. Giles, and S. Garrett-Roe, "Rotationally-resolved two-dimensional infrared spectroscopy of CO_2(g): Rotational wavepackets and angular momentum transfer," J. Phys. Chem. Lett. **13**, 8185–8191 (2022).
[75] G. Kowzan and T. K. Allison, "Theory of rotationally-resolved two-dimensional infrared spectroscopy," arXiv:2206.10488 (2022).
[76] G. Kowzan and T. K. Allison, "Controlling rotationally-resolved two-dimensional infrared spectra with polarization," arXiv:2206.10492 (2022).
[77] NIST Chemistry WebBook, National Institute of Standards and Technology, Gaithersburg, MD.
[78] G. Herzberg, *Infrared and Raman Spectroscopy of Polyatomic Molecules* (Van Nostrand, New York, 1954).
[79] J. Shattuck, P. Shah, S. Erramilli, and L. D. Ziegler, "Structure making and breaking effects of cations in aqueous solution: Nitrous oxide pump–probe measurements," J. Phys. Chem. B **120**, 10569–10580 (2016).
[80] J. T. Shattuck, J. R. Schneck, L. R. Chieffo, S. Erramilli, and L. D. Ziegler, "Dispersed three-pulse infrared photon echoes of nitrous oxide in water and octanol," J. Phys. Chem. B **117**, 15774–15785 (2013).
[81] H. E. Stanley, *Introduction to Phase Transitions and Critical Phenomena* (Oxford University Press, New York, 1971).
[82] J. G. Kirkwood, "Theory of solutions of molecules containing widely separated charges with special application to zwitterions," J. Chem. Phys. **2**, 351–361 (1934).
[83] K. S. Schweizer and D. Chandler, "Vibrational dephasing and frequency shifts of polyatomic molecules in solution," J. Chem. Phys. **76**, 2296–2314 (1982).
[84] G. G. Yee, J. L. Fulton, and R. D. Smith, "Fourier transform infrared spectroscopy of molecular interactions of heptafluoro-1-butanol or 1-butanol in supercritical carbon dioxide and supercritical ethane," J. Phys. Chem. **96**, 6172–6181 (1992).
[85] J. H. Hazzard, J. C. Gorga, and W. S. Caughey, "Determination of anesthetic molecule environments by infrared spectroscopy: II. Multiple sites for nitrous oxide in proteins, lipids, and brain tissue," Arch. Biochem. Biophys. **240**, 747–756 (1985).
[86] J. C. Gorga, J. H. Hazzard, and W. S. Caughey, "Determination of anesthetic molecule environments by infrared spectroscopy. I. Effects of solvating molecule structure on nitrous oxide spectra," Arch. Biochem. Biophys. **240**, 734–746 (1985).
[87] S. A. Egorov, A. Yethiraj, and J. L. Skinner, "Local density enhancement in dilute supercritical solutions," Chem. Phys. Lett. **317**, 558–566 (2000).
[88] P. Hamm and M. T. Zanni, *Concepts and Methods of 2D Infrared Spectroscopy* (Cambridge University Press Cambridge, 2011).
[89] K. Kwak, S. Park, I. J. Finkelstein, and M. D. Fayer, "Frequency-frequency correlation functions and apodization in two-dimensional infrared vibrational echo spectroscopy: A new approach," J. Chem. Phys. **127**, 124503 (2007).
[90] R. Kubo, *Advances in Chemical Physics* (John Wiley & Sons, 2007), pp. 101–127.
[91] S. Mukamel, *Nonlinear Optical Spectroscopy* (Oxford University Press, Oxford, 1995).
[92] T. G. Winter and G. L. Hill, "High-temperature ultrasonic measurements of rotational relaxation in hydrogen, deuterium, nitrogen, and oxygen," J. Acoust. Soc. Am. **42**, 848–858 (1967).
[93] R. N. Healy and T. S. Storvick, "Rotational collision number and Eucken factors from thermal transpiration measurements," J. Chem. Phys. **50**, 1419–1427 (1969).
[94] G. Ganzi and S. I. Sandler, "Determination of thermal transport properties from thermal transpiration measurements," J. Chem. Phys. **55**, 132–140 (1971).
[95] F. Robben and L. Talbot, "Experimental study of the rotational distribution function of nitrogen in a shock wave," Phys. Fluids **9**, 653–662 (1966).
[96] H. P. Broida and T. Carrington, "Rotational, vibrational, and electronic energy transfer in the fluorescence of nitric oxide," J. Chem. Phys. **38**, 136–147 (1963).
[97] C. J. Jameson, A. K. Jameson, and K. Buchi, "Nuclear spin relaxation studies of the spin-rotation interaction of ^{13}C in CO in various buffer gases," J. Chem. Phys. **85**, 697–700 (1986).
[98] T. Umecky, M. Kanakubo, and Y. Ikushima, "^{9}Be NMR relaxation measurements of bis(acetylacetonato)beryllium(II) in liquid and supercritical carbon dioxide: A clear evidence of near-critical solvation effect on rotational correlation time," J. Phys. Chem. B **106**, 11114–11119 (2002).
[99] T. Yamaguchi, N. Matubayasi, and M. Nakahara, "NMR study on the reorientational relaxation in supercritical alcohols," J. Phys. Chem. A **108**, 1319–1324 (2004).
[100] J. C. McCoubrey and W. D. McGrath, "Energy transfer in gaseous collisions," Q. Rev., Chem. Soc. **11**, 87–108 (1957).
[101] G. Maroulis, "Hexadecapole moment, dipole and quadrupole polarizability of sulfur hexafluoride," Chem. Phys. Lett. **312**, 255–261 (1999).
[102] D. Chandler, "Translational and rotational diffusion in liquids. I. Translational single-particle correlation functions," J. Chem. Phys. **60**, 3500–3507 (1974).
[103] D. Chandler, "Rough hard sphere theory of the self-diffusion constant for molecular liquids," J. Chem. Phys. **62**, 1358–1363 (1975).

[104]O. Kravchenko and M. Thachuk, "The effect of rotational and translational energy exchange on tracer diffusion in rough hard sphere fluids," J. Chem. Phys. **134**, 114310 (2011).
[105]D. Chandler, "Translational and rotational diffusion in liquids. II. Orientational single-particle correlation functions," J. Chem. Phys. **60**, 3508–3512 (1974).
[106]K.-i. Saitow, D. Kajiya, and K. Nishikawa, "Dynamics of density fluctuation of supercritical fluid mapped on phase diagram," J. Am. Chem. Soc. **126**, 422–423 (2004).
[107]M. W. Maddox, G. Goodyear, and S. C. Tucker, "Effect of critical slowing down on local-density dynamics," J. Phys. Chem. B **104**, 6266–6270 (2000).
[108]T. N. Olney, N. M. Cann, G. Cooper, and C. E. Brion, "Absolute scale determination for photoabsorption spectra and the calculation of molecular properties using dipole sum-rules," Chem. Phys. **223**, 59–98 (1997).
[109]M. Gussoni, M. Rui, and G. Zerbi, "Electronic and relaxation contribution to linear molecular polarizability. An analysis of the experimental values," J. Mol. Struct. **447**, 163–215 (1998).
[110]R. A. Svehla, NASA Technical Report No. R-132, Lewis Research Center, Cleveland, OH, 1962.
[111]J. O. Hirschfelder, C. F. Curtiss, and R. B. Bird, *Molecular Theory of Gases and Liquids* (Wiley, New York, 1954).
[112]D. W. Breck, *Zeolite Molecular Sieves: Structure, Chemistry, and Use* (Wiley, New York, 1974).
[113]S. Matteucci, Y. Yampolskii, B. D. Freeman, and I. Pinnau, *Materials Science of Membranes for Gas and Vapor Separation* (John Wiley & Sons, 2006), pp. 1–47.
[114]R. A. Svehla, NASA Technical Report No. R-132, Lewis Research Center, Cleveland, OH, 1962.